NURETH14-590

CFD SIMULATION OF ADIABATIC TWO-PHASE FLOW IN THE CAP BUBBLE REGIME USING THE TWO-GROUP INTERFACIAL AREA TRANSPORT EQUATIONS (IATE)

D. Prabhudharwadkar¹, M. Lopez de Bertodano¹, J. Buchanan², P. Guilbert³

¹School of Nuclear Engineering, Purdue University, West Lafayette, Indiana, USA.

²Bechtel Marine Propulsion Corporation, Bettis Laboratory, West Mifflin, Pennsylvania, USA.

³ANSYS UK Ltd., West Central 127, Milton Park, Abingdon, Oxon, UK.

dprabhud@purdue.edu, bertodan@purdue.edu, Jack.Buchanan@unnpp.gov,

paul.guilbert@ansys.com

Abstract

A multidimensional three-field two-fluid model with the two-group IATE is implemented for the bubbly-cap bubble regime. The mechanisms of the two-group IATE bubble interactions that have been proposed and validated in the past for one dimension are extended to a multi-dimensional model. The CFD simulations were validated using the data of Sun et al. [1] where the phase distribution, interfacial area concentration and velocity distribution in the cross-section for the two bubble groups were measured using the four-sensor conductivity probe at four axial locations. The results demonstrate the applicability of the two-group IATE model in three dimensions.

Introduction

The CFD simulation of two-phase flow requires accurate modelling of interfacial mass, momentum and energy transfer. The interfacial transfer term is modelled as a product of the interfacial flux and the interfacial area per unit volume, i.e., the interfacial area concentration. Recent advances in the interfacial area concentration modelling have been focused on the development of the interfacial area transport equation (IATE) which is based on the bubble number density transport equation [2]. The interfacial area transport equation accounts for loss or gain of interfacial area due to coalescence or break-up respectively. The interfacial area concentration provides closure for the bubble size which in turn determines the constitutive relations to be used for the interfacial momentum and energy flux terms, e.g., the drag coefficient. However, in some cases it is necessary to treat different groups of bubbles separately. A onegroup interfacial area transport equation is used for low gas flux, mono-dispersed bubbly flows where the bubbles are in the distorted spherical regime. With higher gas flow rates, the cap bubbles start appearing and a mixture of cap and distorted spherical bubbles requires a two-group interfacial area transport equation to treat the bubble interaction processes for each bubble group separately and also a three-field two-fluid model where each of the bubble groups has a separate mass and momentum conservation equations to handle separate mechanisms of mass and momentum exchange to the continuous fluid and between the two groups. The model is discussed in detail in the next section. The current study is focused on the assessment of the turbulent dispersion forces acting on the bubbles [3] and also on a new model for the displacement force exerted by the faster moving cap bubbles on the small bubbles. It is also the first multidimensional CFD benchmarking effort for the two-group interfacial area transport equation with all the inter and intra-group interaction mechanisms proposed by Sun et al. [4].

1. The Two-Fluid model

The two-fluid model with two-group IATE has been described in detail by Hibiki and Ishii [5]. The mass and momentum equations for each group of bubbles are written separately since the interfacial momentum sources are different for each group. The phase-continuity equation accounts for any inter-group mass transfer of bubbles due to break-up of big bubbles into small bubbles, coalescence of small bubbles into cap bubble or expansion of a small bubble into a cap bubble as it moves through a long channel having significant gas density variations. The continuity equation is thus given as,

$$\frac{\partial}{\partial t} \alpha_k \rho_k + \nabla \cdot \alpha_k \rho_k \underline{\underline{\upsilon}}_k = \begin{cases} 0, & k = 0 \\ -\Delta \dot{m}_{12}, & k = 1 \\ \Delta \dot{m}_{12}, & k = 2 \end{cases}$$
 (1)

where, k=0 is for liquid, k=1 is for small bubbles and k=2 is for the big cap bubbles. α_k stands for the local volume fraction of phase k, ρ_k is the density and $\overline{\varrho}_k$ is the averaged velocity. $\Delta \dot{m}_{12}$ represents the mass transfer rate from Group 1 to 2 per unit mixture volume and it is given by:

$$\Delta \dot{m}_{12} = \frac{\rho_g}{1 + \chi D_{c1}^{*3}} \left[\sum_{j} \eta_j + \eta_{EXP} \right]$$
 (2)

where, η_j is the volume source for the Group II bubbles due to inter-group transfer occurring because of the particle interactions, whereas η_{EXP} is the volume source for Group 2 bubbles because of the expansion of the Group 1 bubbles near the boundary between Group 1 and 2. χ is the inter-group transfer coefficient (= 0.01 in the present simulations) and D_{c1}^* is the dimensionless particle size at the group boundary. The detailed expressions for η_j for each bubble interaction mechanism, η_{EXP} and D_{c1}^* can be found in [4]. The momentum conservation equation for the individual phases is given below.

$$\frac{\partial}{\partial t} \alpha_{k} \rho_{k} \, \underline{\overline{\upsilon}}_{k} + \nabla \cdot \alpha_{k} \rho_{k} \, \underline{\overline{\upsilon}}_{k} \, \underline{\overline{\upsilon}}_{k} = -\alpha_{k} \nabla \rho_{k} + \nabla \cdot \alpha_{k} \left(\underline{\tau}_{k} + \underline{\tau}_{k}^{Re} \right) + \alpha_{k} \rho_{k} \, \underline{g} + \underline{M}_{ki}$$
 (3)

where $\underline{\tau}_{k}^{\text{Re}}$ represents turbulent Reynolds stresses which are closed using the Standard k-epsilon model [3]. \underline{M}_{ki} is the interfacial momentum transfer (i.e., interfacial forces per unit volume). The interfacial forces considered here are the drag on the bubbles [6] and the turbulent dispersion forces. Other interfacial forces such as the lift and the wall force were found to be negligible in this case [3] compared to the dispersion forces. The forces proposed by Lopez de Bertodano et al. [3] for the cap bubbly flow where the interaction of the eddies generated by the cap bubbles with the cap and the small bubbles were considered are included here. The turbulent dispersion force for the cap bubbles is given as follows:

$$M_{BI2}^{TD} = \frac{3}{4} C_{DB2} C_{D2} \rho_0 \langle \alpha_2 \rangle v_{R2}^2 \nabla \alpha_2$$

$$\tag{4}$$

where $\langle \alpha_2 \rangle$ is the cross-sectional average of the volume fraction of the cap bubbles. The turbulent dispersion of the small bubbles induced by the turbulence of the cap bubbles is given by:

$$M_{BI1}^{TD} = \frac{3}{4} C_{DB1} C_{D1} \rho_0 \frac{D_{b2}}{D_{b1}} \langle \alpha_2 \rangle \upsilon_{R2} \upsilon_{R1} \nabla \alpha_1$$
 (5)

The proposed [3] values for C_{DBI} and C_{DB2} were 2.1 and 0.63 respectively based on the simulation performed for a case where $\langle \alpha_2 \rangle \sim 0.05$. $C_{D2} = 3.0$ and $C_{DI} = 2.0$ were proposed by Lopez de Bertodano et al. [3] based on Gaudin's correlation [7]. The small bubbles also interact with eddies that are smaller than the cap bubble sizes and those are generated by shear-induced turbulence. The Lopez de Bertodano model [8] was used for this force with the recommended coefficient value of $C_{TD} = 0.5$.

$$\underline{M}_{1}^{TD} = -C_{TD} \, \rho_{1} k_{1} \nabla \, \alpha_{1} \tag{6}$$

Lopez de Bertodano et al. [9] also proposed a "displacement" force by cap bubbles on the small bubbles which push the small bubbles in the lateral direction when a cap bubble passes through a swarm of small bubbles. Such a displacement was illustrated by Lopez de Bertodano et al. [9] by performing a transient two-fluid model simulation (with only liquid and small bubbles as transported fluids) around an ensemble of fixed cap bubbles. This force is given as follows:

$$M_{Dis1} = -\frac{3}{4} C_{Dis1} C_{D1} \rho_0 \alpha_1 \frac{D_{b2}}{D_{b1}} \nu_{R2} \nu_{R1} \nabla \alpha_2$$
 (7)

 C_{Dis1} was evaluated based on the simulations performed here. The earlier reported calculations for the assessment of the forces acting on the small bubbles did not include the liquid induced turbulent dispersion force given in Eq. (6) and hence in the present study these force coefficients were evaluated again.

2. The two-group Interfacial Area Transport Equation

Sun et al. [4] have proposed the two-group interfacial area transport equation which accounts for the bubble interactions within a group and also between two groups. The IATE is given as follows:

$$\frac{\partial a_{i,k}}{\partial t} + \nabla \cdot \left(\underline{\overline{\nu}}_k a_{i,k} \right) = \phi_{EXP,k} + \sum_j \phi_{j,k} \quad , k = 1, 2$$
 (8)

with $\phi_{EXP,k}$ being the expansion source and $\phi_{j,k}$ being the break-up or coalescence term. The bubble interaction terms are summarized in brief in the table below. However, the detailed description of the model and the coefficients used can be found in [4, 10], where the model coefficients were proposed based on the one-dimensional area averaged modeling approach. In the table below the right column indicates the interacting bubble groups and the product bubble group written in a form analogous to a chemical reaction. All the terms in the table shown below were implemented in the CFD code ANSYS CFX (version 12.1) via user routines [11] and a custom executable was used for the IATE.

Table 1: List of intra and inter-group interaction mechanisms

Mechanism	Type of Interaction	
Random Collision (RC)	$(1)+(1) \rightarrow (1)$ (Sink for Group 1)	
	$(1)+(1)\rightarrow(2)$ (Source for Group 2, Sink for Group 1)	
	$(1)+(2)\rightarrow(2)$ (Sink for Group 1 and 2)	
	$(2)+(2)\rightarrow(2)$ (Sink for Group 2)	
Wake Entrainment (WE)	$(1)+(1)\rightarrow(1)$ (Sink for Group 1)	
	$(1)+(1)\rightarrow(2)$ (Source for Group 2, Sink for Group 1)	
	$(1)+(2)\rightarrow(2)$ (Sink for Group 1 and 2)	
	$(2)+(2)\rightarrow(2)$ (Sink for Group 2)	
Turbulent Impact (TI)	$(1)\rightarrow(1)+(1)$ (Source for Group 1)	
	$(2)\rightarrow(1)+(1)$ (Source for Group 1, Sink for Group 2)	
	$(2)\rightarrow(1)+(1)$ (Source for Group 1)	
	$(2)\rightarrow(2)+(2)$ (Source for Group 2)	
Shearing-Off (SO)	$(2)\rightarrow(2)+(1)$ (Source for Group 1, Sink for Group 2)	
Surface Instability (SI)	$(2)\rightarrow(2)+(2)$ (Source for Group 2)	

3. Description of the experiments and the problem inputs

Figure 1 shows a schematic diagram of the experimental facility and the computational domain. The facility was operated at atmospheric pressure. An acrylic test section with a narrow rectangular cross-section of 200×10 mm was used. Six local measurement ports were installed in the side at different elevations along the test section. The z/D_h values from Port 1 to Port 6 were 8.0, 34.8, 61.5, 88.2, 115.0, and 141.7 respectively. At each port, a state-of-the-art miniaturized four-sensor conductivity probe was traversed in both directions in the cross section of the test section to obtain the local data. The measurement accuracy of ±7 % was reported for the void fraction and interfacial area concentration. The air-water two-phase mixture was injected through

the central one-third region of the inlet and the rest of the inlet being only liquid. Table 2 summarizes the tests simulated here that were reported by Sun et al. [1].

The domain that was simulated here was a quarter of the cross section with two walls and two symmetry boundaries as shown in Fig. 1. The cross-section $(x \times y)$ was 100 mm \times 5 mm and the total length of 2700 mm (up to Port 4) was included for the computations. The mesh was hexahedral with $15\times5\times81$ elements in the width (x), span (y) and length (z) directions respectively after a satisfactory mesh sensitivity test.

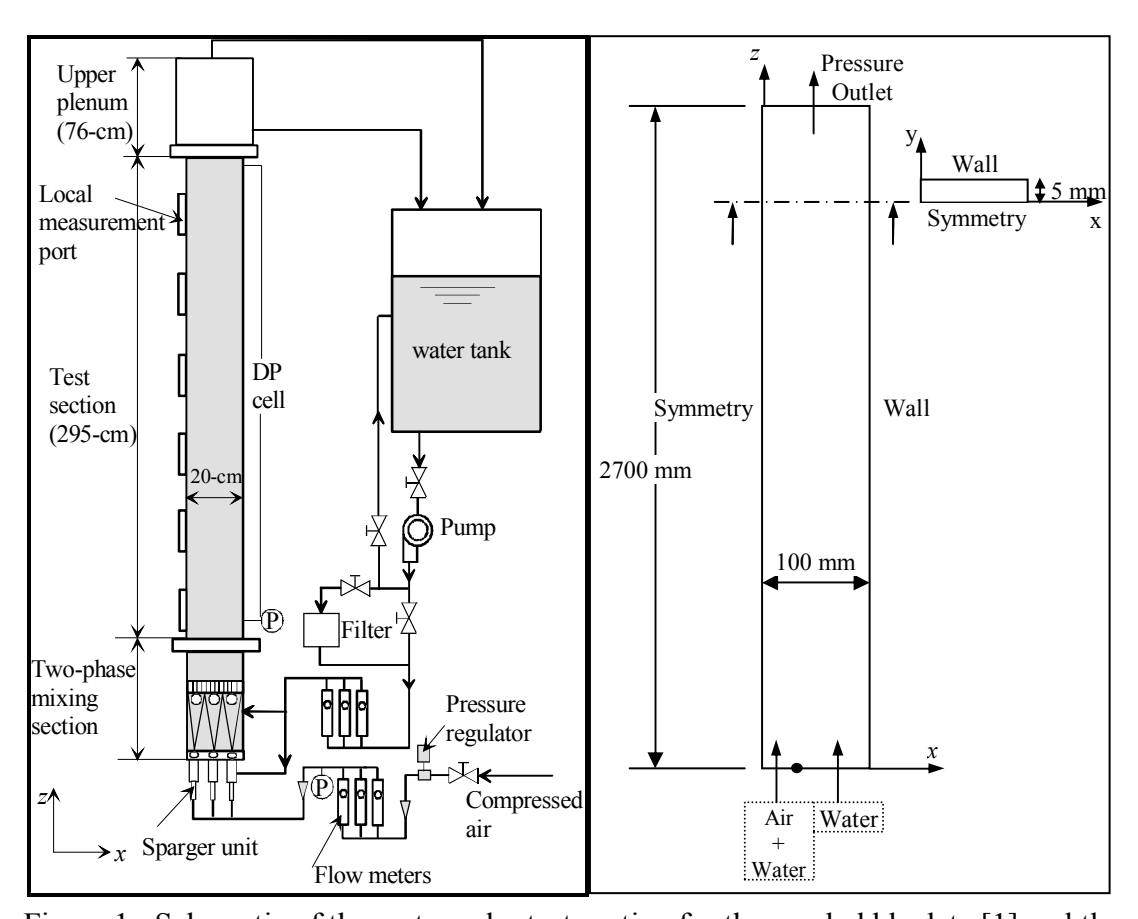


Figure 1 Schematic of the rectangular test section for the cap-bubbly data [1] and the computational domain

Table 2: Flow conditions for the tests simulated

Run	$j_{\rm L}$ (m/s)	j _g (m/s)	Pressure at Port 4 (Pa)
1	0.946	0.095	1.063×10^{5}
2	0.946	0.190	1.055×10^5

Note that the above mentioned gas superficial velocity is based on the total cross-section of the channel and the superficial velocity in the inlet region is approximately three times the above given values since the inlet occupies one third of the total cross-section. The simulation results are discussed in detail in the next section.

4. Results

The previous study [3] on the cap-bubbly jet data focused on the validation of the dispersion forces for each group using the constant bubble diameter simulations which were carried out for Run 2 listed in Table 2. In addition to the dispersion forces, the displacement force acting on the small bubbles due to the faster moving cap bubbles was also tested using Run 2 [9]. The previous calculations were performed with fixed bubble sizes since the data showed no net change in the area averaged void fraction and interfacial area concentration of the individual groups along the length of the test section. Hence, this case was simulated first to check if the previously validated force models need any further modifications owing to the IATE implementation. Then the new capability to model the transport of the interfacial area concentration allowed the simulation of Run 1 in the present study.

4.1 Run 2: $j_L = 0.946$ m/s, $j_g = 0.19$ m/s

Figure 2 shows the volume fractions for both the groups which show a reasonable prediction accuracy of the current model. All the profiles are along the longer axis of the cross-section (i.e., x-axis in Fig. 1) at ports 2 and 6 ($z/D_h \sim 35$ and 142). The group 1 void fractions reported here are with a displacement force coefficient of 0.25. In order to test the influence of the displacement force on the small bubble distribution, calculations were performed without the displacement force and compared with the results with $C_{Dis1} = 0.25$ as shown in Fig. 3. It can be seen that the influence of the displacement force is significant and a coefficient value of 0.25 provides the best estimate at the downstream location. The upstream location prediction with the displacement force is not so good. However it is very close to the inlet and the small bubbles may not have interacted with the big bubbles causing lesser displacement than that predicted by the model. In such case this would be a shortcoming of the two-fluid model averaging rather than of the displacement force model itself. Also, the inlet boundary condition used for both the groups is a constant inlet void fraction, which in reality may be different. The inlet distribution of void will have significant effect on the distribution at port 2. This effect will be less on the fully developed condition at port 6. Figure 4 shows the predictions of the interfacial area concentrations of the two groups which are consistent with the void fraction predictions.

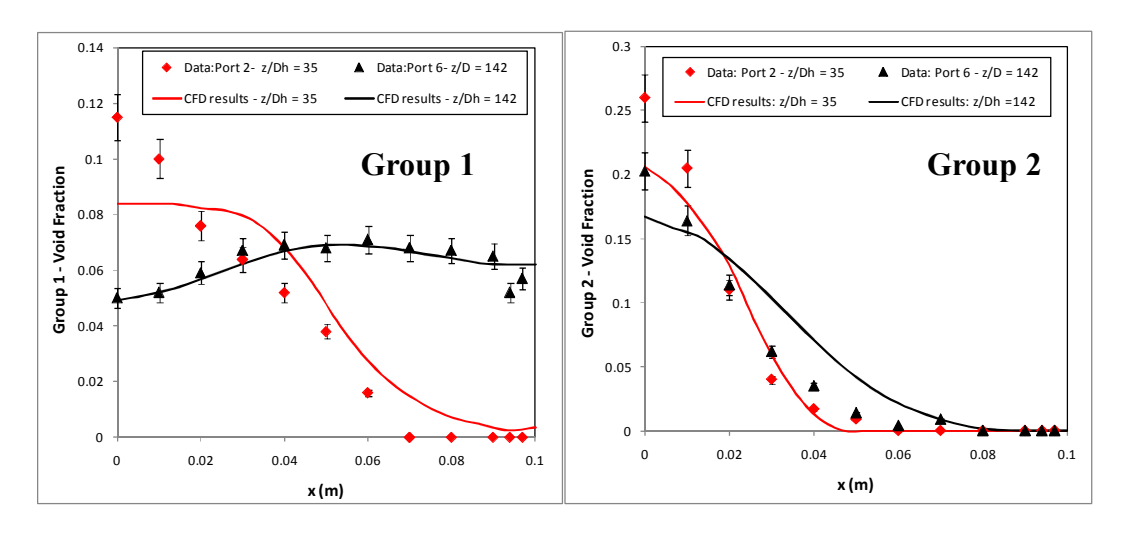


Figure 2 Volume fractions for group 1 and 2 - Run 2

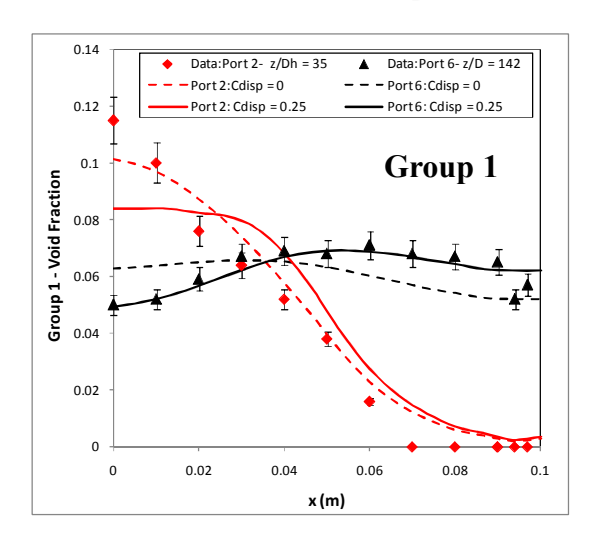


Figure 3 Effect of displacement force on the Volume fractions for group 1 - Run 2

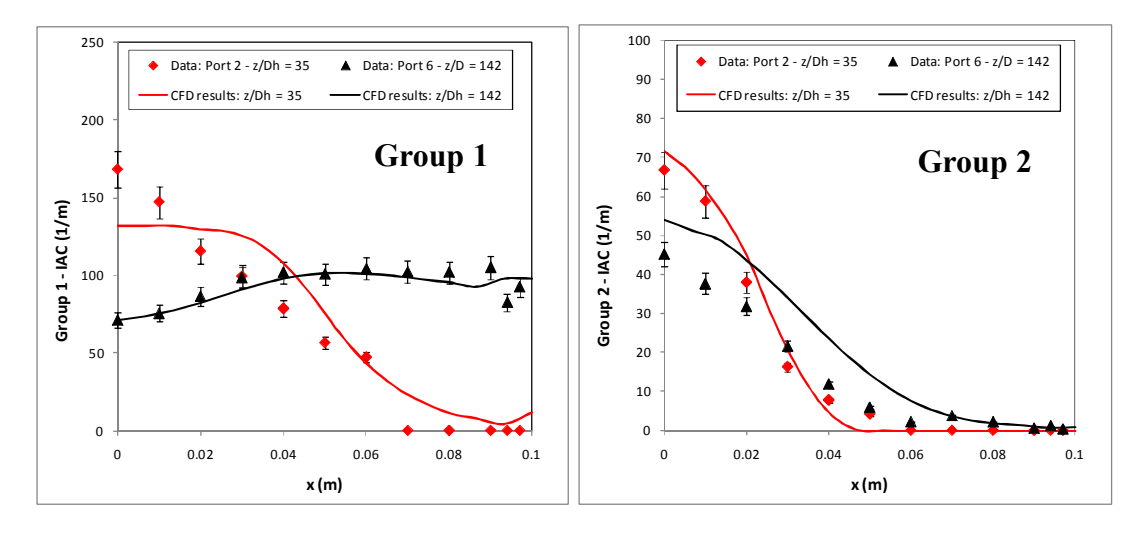


Figure 4 IAC predictions for Run 2

4.2 Run 1: $j_L = 0.946$ m/s, $j_g = 0.095$ m/s

This case is more complicated than the previous one since it starts from the bubbly and cap-bubbly regime boundary at the inlet and the cap bubbles diminish as the jet expands into the bubbly regime [1]. Figure 5 shows the volume fractions of the group 1 bubbles. The results with the current turbulent dispersion model settings are shown by the dashed lines. It was found that the small bubbles had lesser dispersion with the bubble dispersion model of Lopez de Bertodano [3] given by Eq. (5) when used with the suggested coefficient values. The proposed [3] value for C_{DBI} (2.1) was based on the simulation performed for a case where $\langle \alpha_2 \rangle \sim 0.05$. From the calculations performed in this study for two different flow conditions, it revealed that the product C_{DBI} $\langle \alpha_2 \rangle$ turns out to be a constant (i.e., 0.1). The model was hence modified as follows:

$$M_{BI1}^{TD} = \frac{3}{4} C_{DB1,new} C_{D1} \rho_0 \frac{D_{b2}}{D_{b1}} \nu_{R2} \nu_{R1} \nabla \alpha_1$$
(9)

In the above equation, $C_{DBI,new} = 0.1$. The results with the modified model are shown in Fig. 5 by solid lines. The modified model provides sufficient dispersion of the small bubbles especially at the downstream measurement location.

Figure 6 shows the volume fraction of group 2 bubbles. It is visible that the model is not able to predict the significant reduction in the group 2 volume fraction due to transfer to group 1. When the volume sources for group 2 were examined (Fig. 7), it was found that there was a net transfer to group 2 from group 1 due to the expansion effect and the necessary mechanism to generate small bubbles from the cap bubbles was missing.

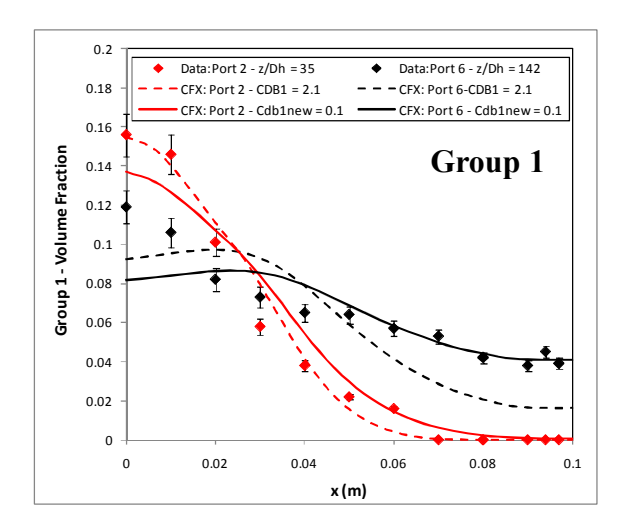


Figure 5 Volume fraction predictions for group 1 using the existing and the modified turbulent dispersion model – Run 1

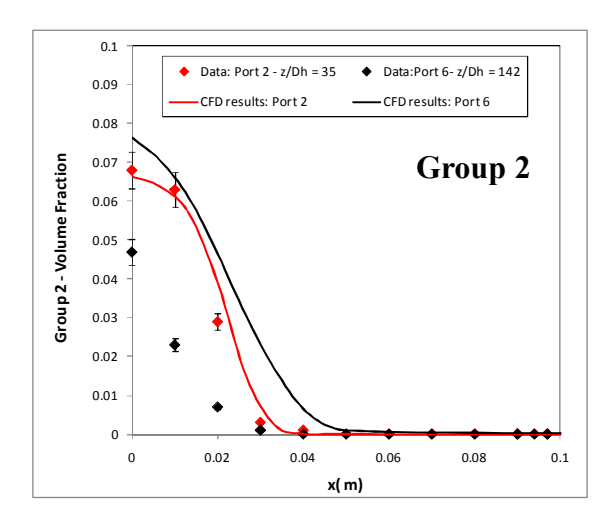


Figure 6 Volume fraction predictions for group 2 – Run 1

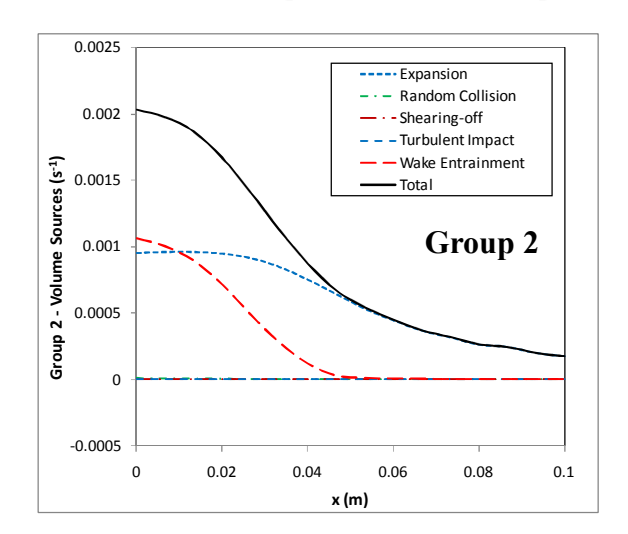


Figure 7 Group 2 volume sources – Run 1

When the group 2 bubble size measurements reported by Sun et al. [1] for this case were studied, it was found that the bubble size (Sauter Mean Diameter) for group 2 bubbles for this case are very close to or lower than the transition between distorted bubbles (group 1) and cap bubbles (group 2) given by,

$$D_{d,\text{max}} = 4\sqrt{\frac{\sigma}{g\Delta\rho}} = 0.0109 \, m \sim 11 \, mm \tag{10}$$

This is shown in Fig. 8 below. Based on this observation an additional transition term due to shearing-off was formulated. The shearing-off mechanism proposed by Sun et al. [4] assumes that the small bubbles are sheared from the cap bubble and the cap bubble is big enough to remain a cap bubble even after shearing-off (i.e., $SO^{2,12} = 2 \rightarrow 2+1$). However, if the cap bubble size is close to the transition to distorted bubbles (group-1), then the shearing-off may result in a cap

bubble reducing to a group-1 (distorted bubble) ($SO^{2,11} = 2 \rightarrow 1+1$). This new term ($SO^{2,11}$) is based on the same concept as Sun et al.'s [4] $SO^{2,12}$ term which is formulated as follows:

The cap bubbles develop a skirt when the disruptive viscous force at the rim cannot be balanced by the cohesive surface tension force. It is assumed that all the sheared-off bubbles are of the same size (d_s) . The shearing-off mechanism is considered similar to the air entrainment in a plunging jet on a liquid pool at rest for which the entrained bubble size distribution has been well studied. The bubble size for the sheared-off bubbles is given as [4]:

$$d_{s} = C_{d,SO} \left(\frac{\sigma}{\rho_{f}}\right)^{3/5} G^{2/5} \nu_{rb}^{-6/5}$$
(11)

In the above equation, G is the gap of the test section which is 10 mm and $v_{\rm rb}$ is the relative velocity of the cap bubble.

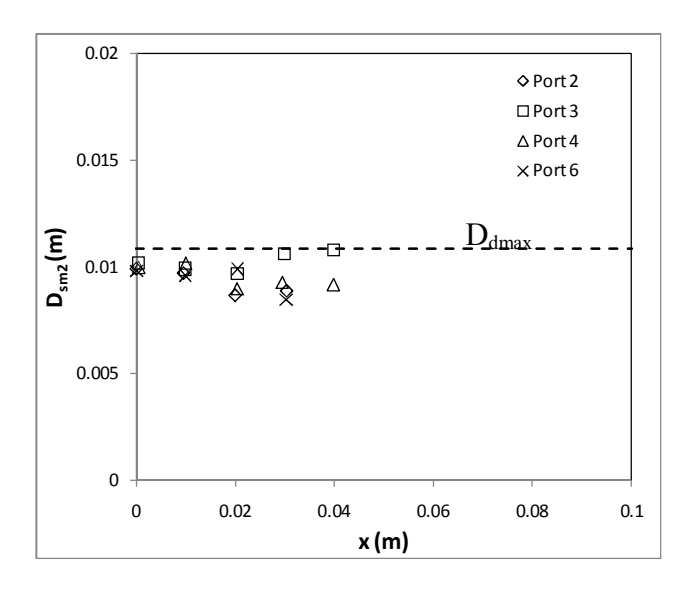


Figure 8 Group 2 bubble size measurements reported by Sun et al. [1]

The number rate (frequency) of small bubbles generated by shearing-off from a large bubble of volume V'[12],

$$\frac{\textit{Volume flow rate of sheared bubbles}}{\textit{Volume of a sheared bubble}} = \frac{Q_{gSO}}{V_{sb}} \propto \frac{V_{\textit{skirt}} / \Delta t}{V_{\textit{sb}}} \propto 9.49 \frac{\upsilon_{\textit{rb}}}{d_s^2 G^{0.5}} V'^{0.5} \tag{12}$$

The rate of change of bubble number density of group 1 by addition of sheared bubbles is obtained by integrating the rate expression for single cap bubble shown above over the entire range of volume of cap bubbles. For the additional shear-off term ($SO^{2,11}$), it is assumed that when a cap bubble with volume between V_c and V_c+V_{sb} is sheared, it will enter the distorted bubble regime which is group 1, where V_{sb} is the volume of a small sheared bubble and V_c is the volume of bubble at the group boundary given by:

$$V_c = 2.6 G \left(\frac{\sigma}{g\Delta \rho} \right) \tag{13}$$

The number density of cap bubbles (number of cap bubbles per unit volume) with volume in the range of V_c and V_c+V_{sb} would be,

$$n_{2,c-s} = \int_{V_c}^{V_c + V_{sb}} f_2 \, dV = \frac{2\alpha_2 \, V_{sb}}{\left(V_{m2}^2 - V_c^2\right)}, \qquad f_2 = \frac{2\alpha_2}{\left(V_{m2}^2 - V_c^2\right)} \tag{14}$$

The above expression is based on the underlying assumption of Sun et. al. [4] that the number density distribution function (f) for both the groups is uniform. V_{m2} is the maximum volume of the cap bubble which is given as,

$$V_{m2} = 0.38 R_{m2}^2 G, R_{m2} = 1.915 D_{sm,2}$$
(15)

The frequency at which the cap bubbles are converted to group 1 bubbles due to shearing is same as the frequency at which the small bubbles shear from the cap bubbles. Number rate (frequency) of small bubbles generated by shearing-off from a large bubble of volume V' is given in Eq. (12) above. The average frequency of shearing for bubbles ranging from V_c and V_c+V_{sb} ,

$$freq \propto \frac{\int_{V_c}^{V_c+V_{sb}} 9.49 \frac{\upsilon_{rb}}{d_s^2 G^{0.5}} V^{\frac{1}{2}} dV}{\int_{V_c}^{V_c+V_{sb}} dV} \propto 9.49 \frac{\upsilon_{rb}}{d_s^2 G^{0.5}} \frac{\frac{2}{3} \left(\left(V_c + V_{sb} \right)^{\frac{3}{2}} - V_c^{\frac{3}{2}} \right)}{V_{sb}}$$
(16)

Hence, the rate (frequency) of change of number density of cap bubbles by shearing-off at the group boundary will be,

$$R_{SO}^{(2,11)} = n_{2,c-s} freq = 12.65 C_{SO21} \frac{\alpha_2 v_{rb}}{d_s^2 G^{0.5}} \frac{\left(\left(V_c + V_{sb} \right)^{\frac{3}{2}} - V_c^{\frac{3}{2}} \right)}{\left(V_{m2}^2 - V_c^2 \right)}$$
(17)

 C_{SO21} needs to be obtained from the simulations. The inter-group volume transport due to bubbles transforming to group 1 with bubble size $D_{d,max}$,

$$\eta_{SO}^{2,11} = -R_{SO}^{(2,11)} \frac{\pi D_{d,\text{max}}^3}{6} \tag{18}$$

The interfacial area concentration source to group 1 and sink to group 2 will be,

$$\phi_{SO1}^{2,11} = R_{SO}^{(2,11)} \pi D_{d \max}^2$$
 (19)

$$\phi_{SO,2}^{2,11} = -R_{SO}^{(2,11)} A_c \tag{20}$$

 A_c is the interfacial area of the cap bubble on the group boundary which is given as follows from the assumed geometry of the cap bubble [4],

$$A_c = 0.76 R_c^2 + 3.28 G R_c, R_c = D_{d,\text{max}} / 2 \sin 50^\circ$$
 (21)

Figure 9 shows the effect of the addition of the new shear-off term on the volume fraction of the cap bubbles. It is seen that the additional term is indeed effective and provides the necessary transfer from group 2 to group 1 when a value of 0.04 is chosen for C_{SO21} . The model is more effective at the downstream location ($z/D_h = 142$). There is no significant transfer in the short distance up to the upstream location ($z/D_h = 35$) and hence no noticeable difference is seen here. Also, note that the addition of this term is a special case since the cap bubble size is very close to the transition to group 1 bubbles. This term did not exist for Run 2 where the cap bubble size is much greater than $D_{d,max}$.

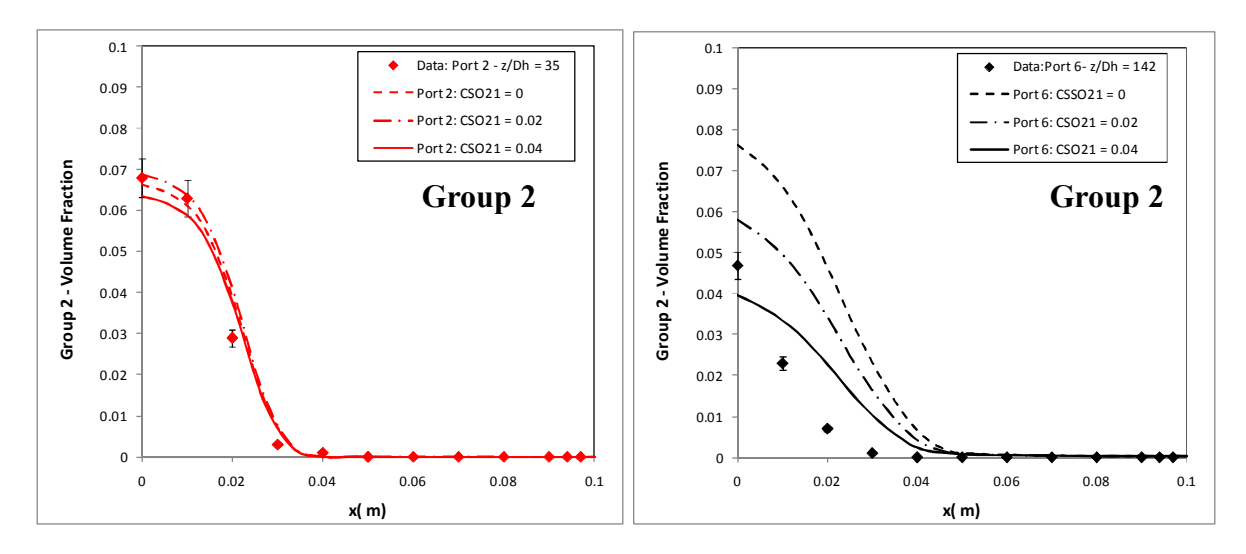


Figure 9 Effect of the new group boundary shear-off term – Run 1

Figure 10 shows the volume fraction of group 1 after addition of the new shearing-off term which has higher values near the axis than in the previous case (Fig. 8) at the downstream location. Note that the simulations were carried out with ($C_{Dis1} = 0.25$) and without the displacement force. It shows that this force is less dominant in this case owing to low group 2 bubble concentration. Predictions at port 2 are more accurate than that at port 6 and the average volume fraction is comparable at both measurement ports. Figure 11 shows the interfacial area concentration predictions which have an accuracy comparable to the respective volume fraction predictions.

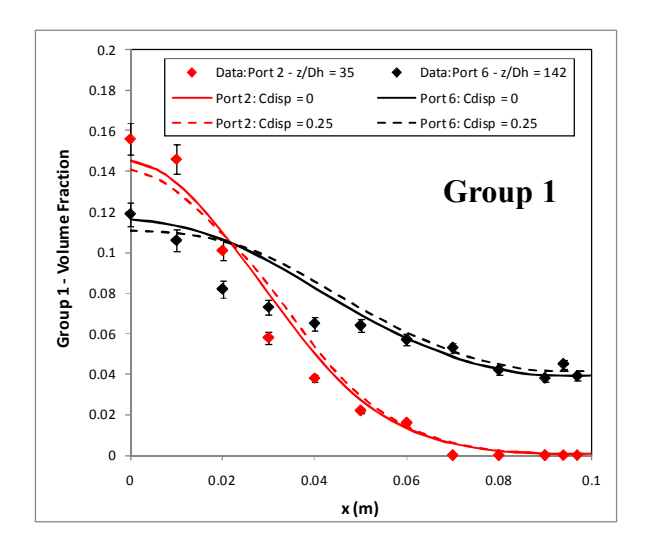


Figure 10 Group 1 volume fraction after addition of new SO term – Run 1

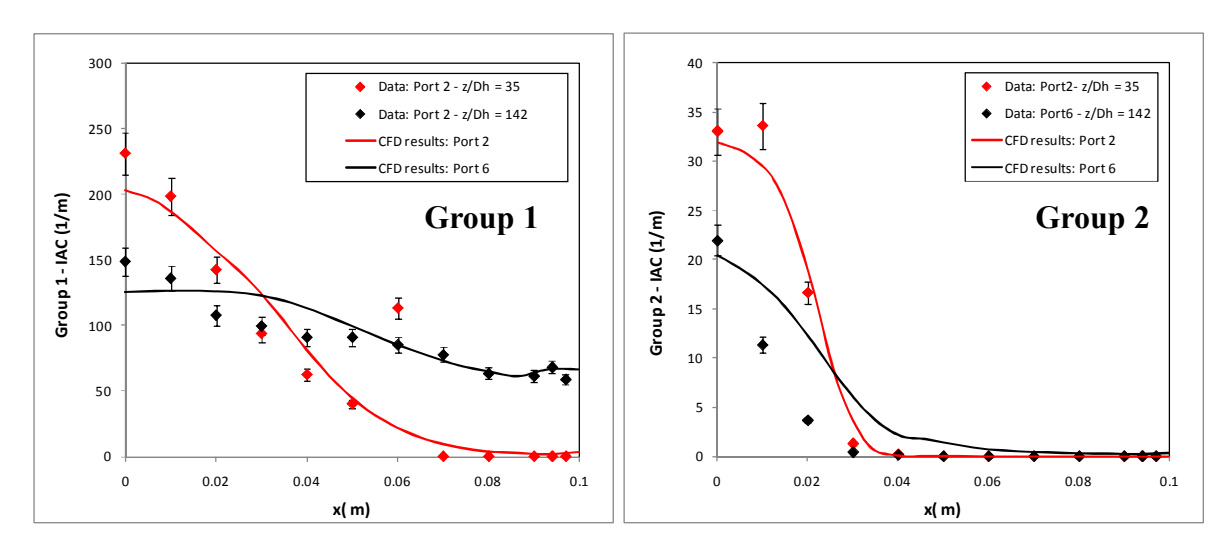


Figure 11 Interfacial area concentration predictions of the two groups - Run 1

5. Conclusions

The three-field, two-fluid model simulations with two-group IATE were performed for the multidimensional cap-bubbly jet data of Sun et al. [1]. From these results it can be concluded that:

1. The turbulent dispersion force models that were previously proposed by Lopez de Bertodano et al. [3] based on constant diameter simulation for Run 2 only were found to be applicable for Runs 1 and 2 using the two-group IATE with varying bubble diameters. However, based on the simultaneous comparisons of runs 1 and 2, the turbulent dispersion force on the small bubbles by the eddies of the big bubbles was modified.

- 2. Run 2 allowed an independent assessment of the displacement force of the cap bubbles as they push the small bubbles to the side. The force could be determined separately of other IATE effects since the IATE source terms balanced out.
- 3. An additional inter-group transfer mechanism was proposed and validated for a special case (encountered in Run 1) where the flow conditions are close to the bubbly to cap bubble transition.

6. References

- [1] Sun, X., Vasavada, S., Choi, S.W., Kim S., Ishii, M., Beus, S. G., 2005, "Interfacial Structure in an Air-Water Planar Bubble Jet", Experiments in Fluids, 38, pp. 426-439.
- [2] Kocamustafaogullari, G. and Ishii, M., 1995, "Foundation of the Interfacial Area Transport Equation and its Closure Relations", International Journal of Heat and Mass Transfer, 38, pp. 481-493.
- [3] Lopez de Bertodano, M.A., Sun, X., Ishii, M., Ulke A., 2006, "Phase Distribution in the Cap Bubble Regime in a Duct", Journal of Fluids Engineering, 128, pp. 811-818.
- [4] Sun, X., Kim, S., Ishii, M., Beus, S., 2004, "Modeling of bubble coalescence and disintegration in confined upward two-phase flow", Nuclear Engineering and Design, 230, pp. 3-26.
- [5] Ishii, M. and Hibiki, T., 2006, *Thermo-Fluid Dynamics of Two-Phase Flow*, Springer, New York, USA.
- [6] Ishii, M. and Zuber N., 1979, "Drag coefficient and relative velocity in bubbly, droplet or particulate flows", AIChE Journal, 25(5), pp. 843-855.
- [7] Gaudin, A. M., 1957, *Flotation*, 2nd ed., Mc–Graw Hill, New York.
- [8] Lopez de Bertodano, M. A., Lahey, Jr., R. T. and Jones, O. C., 1994, "Phase distribution in bubbly two-phase flow in vertical ducts", International Journal of Multiphase Flow, 20(5), pp. 805-818.
- [9] Lopez de Bertodano, M. A., Sun, X., Buchanan, J., 2007, "A Three-Field Two-Fluid CFD Model with a Lateral Displacement Force for the Cap Bubble Regime in a Duct." <u>Proceedings of the 6th International Conference on Multiphase Flow</u>, Leipzig, Germany.
- [10] Sun, X., Kim, S., Ishii, M., and Beus, S. G., 2004, "Model Evaluation of Two-Group Interfacial Area Transport Equation for Confined Upward Flow", Nuclear Engineering and Design, 230, pp. 27–47.
- [11] ANSYS Inc., "ANSYS CFX Solver Theory Guide", ANSYS CFX Release 12.1, 2009.
- [12] Sun X., 2001, "Two-group interfacial area transport equation for a confined test section", Ph.D. Thesis, Purdue University, West Lafayette, USA.